Harmonic decomposition of two particle angular correlations in Pb–Pb collisions at $\sqrt{s_{NN}} = 2.76$ TeV ☆

ALICE Collaboration

A B S T R A C T

Angular correlations between unidentified charged trigger (t) and associated (a) particles are measured by the ALICE experiment in Pb–Pb collisions at $\sqrt{s_{NN}} = 2.76$ TeV for transverse momenta $0.25 < p_T^{t,a} < 15$ GeV/c, where $p_T^t > p_T^a$. The shapes of the pair correlation distributions are studied in a variety of collision centrality classes between 0 and 50% of the total hadronic cross section for particles in the pseudorapidity interval $|\eta| < 1.0$. Distributions in relative azimuth $\Delta\phi \equiv \phi^t - \phi^a$ are analyzed for $|\Delta\eta| \equiv |\eta^t - \eta^a| > 0.8$, and are referred to as "long-range correlations". Fourier components $V_{n\Delta} \equiv \langle\cos(n\Delta\phi)\rangle$ are extracted from the long-range azimuthal correlation functions. If particle pairs are correlated to one another through their individual correlation to a common symmetry plane, then the pair anisotropy $V_{n\Delta}(p_T^t, p_T^a)$ is fully described in terms of single-particle anisotropies $v_n(p_T)$ as $V_{n\Delta}(p_T^t, p_T^a) = v_n(p_T^t)v_n(p_T^a)$. This expectation is tested for $1 \leqslant n \leqslant 5$ by applying a global fit of all $V_{n\Delta}(p_T^t, p_T^a)$ to obtain the best values $v_n\{GF\}(p_T)$. It is found that for $2 \leqslant n \leqslant 5$, the fit agrees well with data up to $p_T^a \sim 3$–4 GeV/c, with a trend of increasing deviation as p_T^t and p_T^a are increased or as collisions become more peripheral. This suggests that no pair correlation harmonic can be described over the full $0.25 < p_T < 15$ GeV/c range using a single $v_n(p_T)$ curve; such a description is however approximately possible for $2 \leqslant n \leqslant 5$ when $p_T^a < 4$ GeV/c. For the $n = 1$ harmonic, however, a single $v_1(p_T)$ curve is not obtained even within the reduced range $p_T^a < 4$ GeV/c.

© 2012 CERN Published by Elsevier. B V   Open access under CC BY-NC-ND license.

1. Introduction

Ultra-relativistic collisions of large nuclei at the Large Hadron Collider (LHC) and at the Relativistic Heavy Ion Collider (RHIC) enable the study of strongly-interacting nuclear matter at extreme temperatures and energy densities. One key piece of evidence for the formation of dense partonic matter in these collisions is the observation of particle momentum anisotropy in directions transverse to the beam [1–6]. One powerful technique to characterize the properties of the medium is with two-particle correlations [7–18], which measure the distributions of angles $\Delta\phi$ and/or $\Delta\eta$ between particle pairs consisting of a "trigger" at transverse momentum p_T^t and an "associated" partner at p_T^a.

In proton–proton collisions, the full $(\Delta\phi, \Delta\eta)$ correlation structure at $(\Delta\phi, \Delta\eta) \approx (0, 0)$ is dominated by the "near-side" jet peak, where trigger and associated particles originate from a fragmenting parton, and at $\Delta\phi \approx \pi$ by the recoil or "away-side" jet. The away-side peak is broader in $\Delta\eta$, due to the longitudinal momentum distribution of partons in the colliding nuclei. In central nucleus–nucleus collisions at RHIC, an additional "ridge" feature is observed at $\Delta\phi \approx 0$ [13,14], which has generated considerable theoretical interest [19–29] since its initial observation. With increasing p_T,

the contribution from the near-side jet peak increases, while the ridge correlation maintains approximately the same amplitude. The recoil jet correlation is significantly weaker than that of the near side, because of kinematic considerations [30] and also because of partonic energy loss. When both particles are at high transverse momenta ($p_T^a \gtrsim 6$ GeV/c), the peak shapes appear similar to the proton–proton case, albeit with a more suppressed away side. This away-side correlation structure becomes broader and flatter than in proton–proton collisions as the particle p_T is decreased. In fact, in very central events (≈ 0–2%), the away side exhibits a concave, doubly-peaked feature at $|\Delta\phi - \pi| \approx 60°$ [31], which also extends over a large range in $|\Delta\eta|$ [17,18]. The latter feature has been observed previously at RHIC [12–14], but only after subtraction of a correlated component whose shape was exclusively attributed to elliptic flow.

However, recent studies suggest that fluctuations in the initial state geometry can generate higher-order flow components [32–40]. The azimuthal momentum distribution of the emitted particles is commonly expressed as

$$\frac{dN}{d\phi} \propto 1 + \sum_{n=1}^{\infty} 2v_n(p_T)\cos\big(n(\phi - \Psi_n)\big) \tag{1}$$

where v_n is the magnitude of the nth order harmonic term relative to the angle of the initial-state spatial plane of symmetry Ψ_n.

First measurements, in particular of v_3 and v_5 have been reported recently [17,31,41].

These higher-order harmonics contribute to the previously-described structures observed in trigger-associated particle correlations via the expression

$$\frac{dN^{\text{pairs}}}{d\Delta\phi} \propto 1 + \sum_{n=1}^{\infty} 2v_n(p_T^t)v_n(p_T^a)\cos(n\Delta\phi). \qquad (2)$$

Similarly, the *measured* anisotropy from two-particle correlations at harmonic order n is given by $V_{n\Delta}$:

$$\frac{dN^{\text{pairs}}}{d\Delta\phi} \propto 1 + \sum_{n=1}^{\infty} 2V_{n\Delta}(p_T^t, p_T^a)\cos(n\Delta\phi). \qquad (3)$$

In this Letter, we present a measurement of the $V_{n\Delta}$ coefficients from triggered, pseudorapidity-separated ($|\Delta\eta| > 0.8$) pair azimuthal correlations in Pb–Pb collisions in different centrality classes and in several transverse momentum intervals. Details of the experimental setup and analysis are described in Sections 2 and 3, respectively. The goal of the analysis is to quantitatively study the connection between the measured two-particle anisotropy $V_{n\Delta}$ of Eq. (3) and the inclusive-particle harmonics of Eq. (2). Specifically, we check whether a set of single-valued $v_n(p_T)$ points can be identified that describe the measured long-range anisotropy via the relation $v_n(p_T^t)v_n(p_T^a) = V_{n\Delta}(p_T^t, p_T^a)$. If so, $V_{n\Delta}$ is said to *factorize* into single-particle Fourier coefficients within the relevant p_T^t, p_T^a region. This relationship is tested for different harmonics n and in different centrality classes by performing a global fit (*GF*) over all $p_T^{t,a}$ bins (see Section 4). The global fit procedure results in the coefficients $v_n\{GF\}(p_T)$ that best describe the anisotropy given by the $V_{n\Delta}(p_T^t, p_T^a)$ harmonics as $v_n\{GF\}(p_T^t) \times v_n\{GF\}(p_T^a)$. The resulting $v_n\{GF\}$ values for $1 < n \leqslant 5$ are presented in Section 5. A summary is given in Section 6.

2. Experimental setup and data analysis

The data used in this analysis were collected with the ALICE detector in the first Pb–Pb run at the LHC (November 2010). Charged particles are tracked using the Time Projection Chamber (TPC), whose acceptance enables particle reconstruction within $-1.0 < \eta < 1.0$. Primary vertex information is provided by both the TPC and the silicon pixel detector (SPD), which consists of two cylindrical layers of hybrid silicon pixel assemblies covering $|\eta| < 2.0$ and $|\eta| < 1.4$ for the inner and outer layers, respectively. Two VZERO counters, each containing two arrays of 32 scintillator tiles and covering $2.8 < \eta < 5.1$ (VZERO-A) and $-3.7 < \eta < -1.7$ (VZERO-C), provide amplitude and time information for triggering and centrality determination. The trigger was configured for high efficiency to accept inelastic hadronic collisions. The trigger is defined by a coincidence of the following three conditions: i) two pixel hits in the outer layer of the SPD, ii) a hit in VZERO-A, and iii) a hit in VZERO-C.

Electromagnetically induced interactions are rejected by requiring an energy deposition above 500 GeV in each of the Zero Degree Calorimeters (ZDCs) positioned at ± 114 m from the interaction point. Beam background events are removed using the VZERO and ZDC timing information. The combined trigger and selection efficiency is estimated from a variety of Monte Carlo (MC) studies. This efficiency ranges from 97% to 99% and has a purity of 100% in the 0–90% centrality range. The dataset for this analysis includes approximately 13 million events. Centrality was determined by the procedure described in Ref. [42]. The centrality resolution, obtained by correlating the centrality estimates of the VZERO, SPD and TPC detectors, is found to be about 0.5% RMS for the 0–10%

most central collisions, allowing centrality binning in widths of 1 or 2 percentiles in this range.

This analysis uses charged particle tracks from the ALICE TPC having transverse momenta from 0.25 to 15 GeV/c. The momentum resolution $\sigma(p_T)/p_T$ rises with p_T and ranges from 1–2% below 2 GeV/c up to 10–15% near 15 GeV/c, with a negligible dependence on occupancy. Collision vertices are determined using both the TPC and SPD. Collisions at a longitudinal position greater than 10 cm from the nominal interaction point are rejected. The closest-approach distance between each track and the primary vertex is required to be within 3.2 (2.4) cm in the longitudinal (radial) direction. At least 70 TPC pad rows must be traversed by each track, out of which 50 TPC clusters must be assigned. In addition, a track fit is applied requiring χ^2 per TPC cluster $\leqslant 4$ (with 2 degrees of freedom per cluster).

3. Two-particle correlation function and Fourier analysis

The two-particle correlation observable measured here is the correlation function $C(\Delta\phi, \Delta\eta)$, where the pair angles $\Delta\phi$ and $\Delta\eta$ are measured with respect to the trigger particle. The correlations induced by imperfections in detector acceptance and efficiency are removed via division by a mixed-event pair distribution $N_{\text{mixed}}(\Delta\phi, \Delta\eta)$, in which a trigger particle from a particular event is paired with associated particles from separate events. This acceptance correction procedure removes structure in the angular distribution that arises from non-uniform acceptance and efficiency, so that only physical correlations remain. Within a given p_T^t, p_T^a, and centrality interval, the correlation function is defined as

$$C(\Delta\phi, \Delta\eta) \equiv \frac{N_{\text{mixed}}}{N_{\text{same}}} \times \frac{N_{\text{same}}(\Delta\phi, \Delta\eta)}{N_{\text{mixed}}(\Delta\phi, \Delta\eta)}. \qquad (4)$$

The ratio of mixed-event to same-event pair counts is included as a normalization prefactor such that a completely uncorrelated pair sample lies at unity for all angles. For $N_{\text{mixed}}(\Delta\phi, \Delta\eta)$, events are combined within similar categories of collision vertex position so that the acceptance shape is closely reproduced, and within similar centrality classes to minimize effects of residual multiplicity correlations. To optimize mixing accuracy on the one hand and statistical precision on the other, the event mixing bins vary in width from 1 to 10% in centrality and 2 to 4 cm in longitudinal vertex position.

It is instructive to consider the two examples of $C(\Delta\phi, \Delta\eta)$ from Fig. 1 to be representative of distinct kinematic categories. The first is the "bulk-dominated" regime, where hydrodynamic modeling has been demonstrated to give a good description of the data from heavy-ion collisions [1–5]. We designate particles with p_T^t (thus also p_T^a) below 3–4 GeV/c as belonging to this region for clarity of discussion (see Fig. 1, left). A second category is the "jet-dominated" regime, where both particles are at high momenta ($p_T^a > 6$ GeV/c), and pairs from the same di-jet dominate the correlation structures (see Fig. 1, right).

A major goal of this analysis is to quantitatively study the evolution of the correlation shapes between these two regimes as a function of centrality and transverse momentum. In order to reduce contributions from the near-side peak, we focus on the correlation features at long range in relative pseudorapidity by requiring $|\Delta\eta| > 0.8$. This gap is selected to be as large as possible while still allowing good statistical precision within the TPC acceptance. The projection of $C(\Delta\phi, |\Delta\eta| > 0.8)$ into $\Delta\phi$ is denoted as $C(\Delta\phi)$.

An example of $C(\Delta\phi)$ from central Pb–Pb collisions in the bulk-dominated regime is shown in Fig. 2 (left). The prominent near-side peak is an azimuthal projection of the ridge seen in Fig. 1. In this very central collision class (0–2%), a distinct doubly-peaked
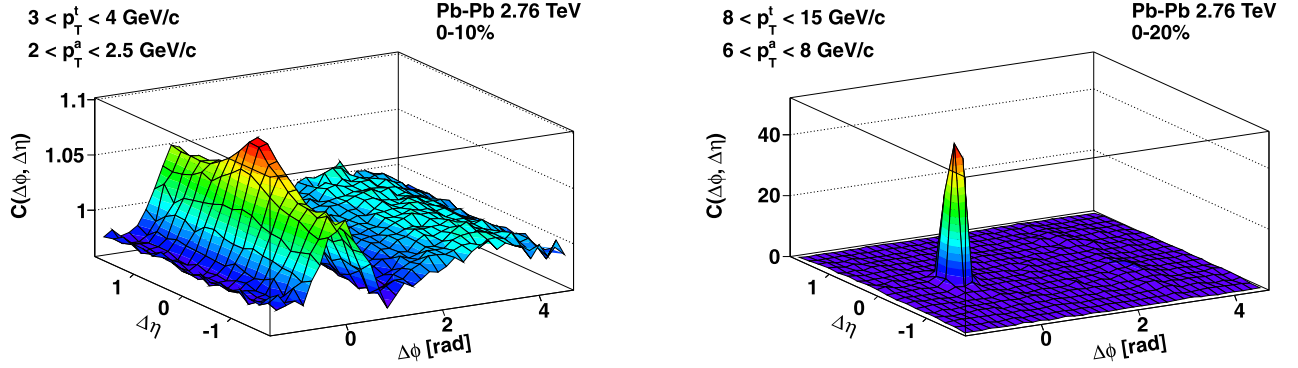
Fig. 1. Examples of two-particle correlation functions $C(\Delta\phi, \Delta\eta)$ for central Pb–Pb collisions at low to intermediate transverse momentum (left) and at higher p_T (right). Note the large difference in vertical scale between panels.
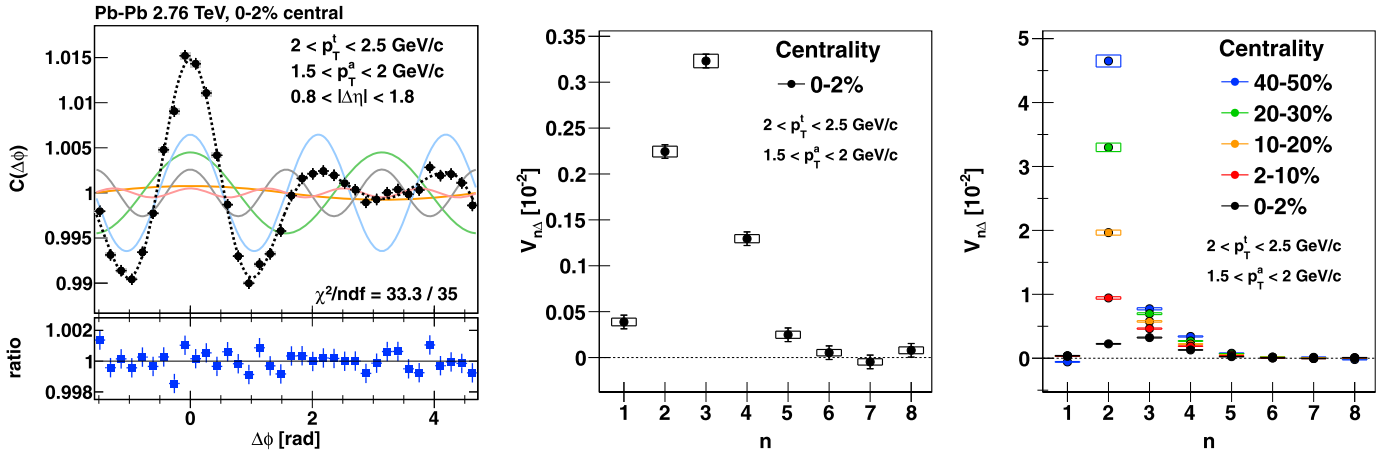

Fig. 2. (Color online.) Left: $C(\Delta\phi)$ for particle pairs at $|\Delta\eta| > 0.8$. The Fourier harmonics for $V_{1\Delta}$ to $V_{5\Delta}$ are superimposed in color. Their sum is shown as the dashed curve. The ratio of data to the $n \leqslant 5$ sum is shown in the lower panel. Center: Amplitude of $V_{n\Delta}$ harmonics vs. n for the same p_T^t, p_T^a, and centrality class. Right: $V_{n\Delta}$ spectra for a variety of centrality classes. Systematic uncertainties are represented with boxes (see Section 4), and statistical uncertainties are shown as error bars.
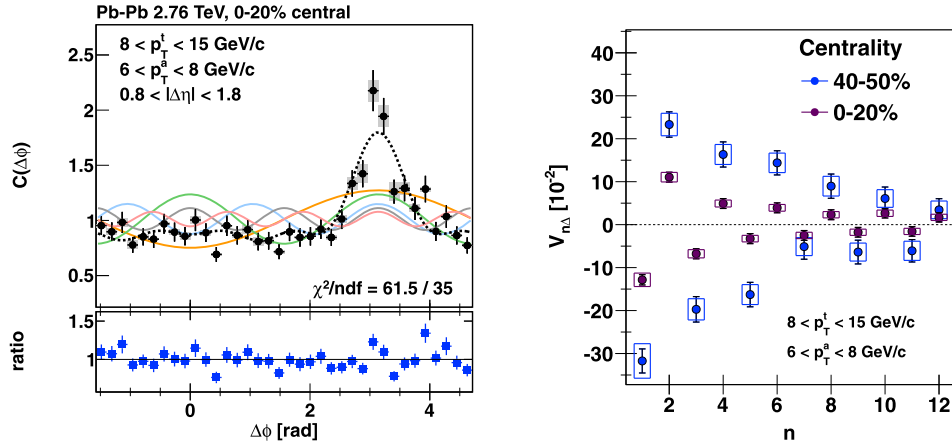

Fig. 3. (Color online.) Left: $C(\Delta\phi)$ at $|\Delta\eta| > 0.8$ for higher-p_T particles than in Fig. 2. The Fourier harmonics $V_{n\Delta}$ for $n \leqslant 5$ are superimposed in color. Their sum is shown as the dashed curve. The ratio of data to the $n \leqslant 5$ sum is shown in the lower panel. Right: Amplitude of $V_{n\Delta}$ harmonics vs. n at the same p_T^t, p_T^a for two centrality bins. Systematic uncertainties are represented with boxes (see Section 4), and statistical uncertainties are shown as error bars.

structure is visible on the away side, which becomes a progressively narrower single peak in less central collisions. We emphasize that no subtraction was performed on $C(\Delta\phi)$, unlike other jet correlation analyses [7–14].

A comparison between the left panels of Fig. 2 and Fig. 3 demonstrates the change in shape as the transverse momentum is increased. A single recoil jet peak at $\Delta\phi \simeq \pi$ appears whose amplitude is no longer a few percent, but now a factor of 2 above unity. No significant near-side ridge is distinguishable at this scale. The recoil jet peak persists even with the introduction of a gap in $|\Delta\eta|$ due to the distribution of longitudinal parton momenta in the colliding nuclei.
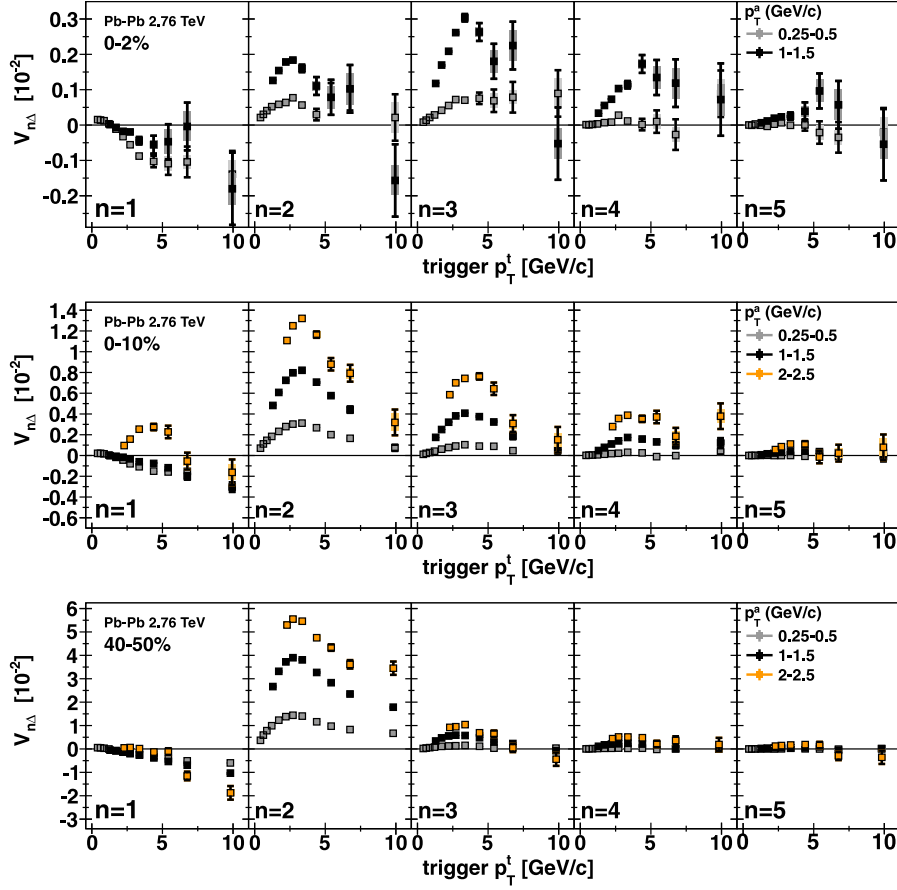
Fig. 4. $V_{n\Delta}$ coefficients as a function of p_T^t for the 0–2%, 0–10%, and 40–50% most central Pb–Pb collisions (top to bottom).

The features of these correlations can be parametrized at various momenta and centralities by decomposition into discrete Fourier harmonics, as done (for example) in [38,40]. Following the convention of those references, we denote the two-particle Fourier coefficients as $V_{n\Delta}$ (see Eq. (3)), which we calculate directly from $C(\Delta\phi)$ as

$$V_{n\Delta} \equiv \langle \cos(n\Delta\phi) \rangle = \sum_i C_i \cos(n\Delta\phi_i) / \sum_i C_i. \qquad (5)$$

Here, C_i indicates that the $C(\Delta\phi)$ is evaluated at $\Delta\phi_i$. Thus $V_{n\Delta}$ is independent of the normalization of $C(\Delta\phi)$. The $V_{n\Delta}$ harmonics are superimposed on the left panels of Fig. 2 and Fig. 3. In the right panels, the $V_{n\Delta}$ spectrum is shown for the same centrality and momenta, with additional centrality classes included to illustrate the centrality dependence. The systematic uncertainties in these figures are explained in Section 4.

In the bulk-dominated momentum regime and for central collisions (Fig. 2), the first few Fourier harmonics are comparable in amplitude, with the notable exception of $V_{1\Delta}$. The first 5 combined harmonics reproduce $C(\Delta\phi)$ with high accuracy, as shown in the ratio between the points and the component sum. For less central collisions, $V_{2\Delta}$ increasingly dominates. In the high-p_T regime (Fig. 3), the jet peak at $\Delta\phi = \pi$ is the only prominent feature of the correlation function. The even (odd) harmonics take positive (negative) values which diminish in magnitude with increasing n, forming a pattern distinct from the low-p_T case. The dependence of the values on n in the left panel of Fig. 3 is approximately consistent with a Gaussian function centered at $n = 0$, as expected for the Fourier transform of a Gaussian distribution of

width $\sigma_n = 1/\sigma_{\Delta\phi}$ centered at $\Delta\phi = \pi$. In this case, the sum of the first 5 harmonics does not reproduce $C(\Delta\phi)$ with the accuracy of the low-p_T case, as suggested by the larger χ^2 value (61.5/35 compared to 33.3/35). Although not shown, it was found that including additional harmonics significantly improves the χ^2/NDF measure for high-p_T^q correlations, but adding higher orders in the bulk-dominated case has only a modest effect. For example, if curves composed of the lowest ten harmonics are used, the χ^2 value drops by only about 10% to 30.0/35 in Fig. 2, but by over 25% to 45.7/35 in Fig. 3. We note that v_2 is not the dominant coefficient in Fig. 3; instead, its magnitude fits into a pattern without significant dependence on collision geometry, as suggested by the continuous decrease with increasing n for both 0–20% and 40–50% central events. This suggests that the n spectrum is driven predominantly by intra-jet correlations on the recoil side, as expected from proton–proton correlations at similar particle momenta.

Fig. 4 shows the $V_{n\Delta}$ coefficients as a function of trigger p_T for a selection of associated p_T values. For $n \geq 2$, $V_{n\Delta}$ reaches a maximum value at $p_T^t \simeq 3$–4 GeV/c, decreasing toward zero (or even below zero for odd n) as p_T^t increases. This rapid drop of the odd coefficients at high p_T^t provides a complementary picture to the n dependence of $V_{n\Delta}$ shown in Fig. 3.

4. Factorization and the global fit

The trends in p_T^t and centrality in Fig. 4 are reminiscent of previous measurements of v_n from anisotropic flow analyses [17,31, 41]. This is expected if the azimuthal anisotropy of final state particles at large $|\Delta\eta|$ is induced by a collective response to initial-state coordinate-space anisotropy from collision geometry and fluctua-

tions [37]. In such a case, $C(\Delta\phi)$ reflects a mechanism that affects all particles in the event, and $V_{n\Delta}$ depends only on the single-particle azimuthal distribution with respect to the nth order symmetry plane Ψ_n. Under these circumstances $V_{n\Delta}$ factorizes as

$$
\begin{aligned}
V_{n\Delta}\left(p_T^t, p_T^a\right) &= \left\langle\!\left\langle e^{in(\phi_a-\phi_t)}\right\rangle\!\right\rangle \\
&= \left\langle\!\left\langle e^{in(\phi_a-\Psi_n)}\right\rangle\!\left\langle e^{-in(\phi_t-\Psi_n)}\right\rangle\!\right\rangle \\
&= \left\langle v_n\{2\}\left(p_T^t\right) v_n\{2\}\left(p_T^a\right)\right\rangle. \qquad (6)
\end{aligned}
$$

Here, $\langle\ \rangle$ indicates an averaging over events, $\langle\!\langle\ \rangle\!\rangle$ denotes averaging over both particles and events, and $v_n\{2\}$ specifies the use of a two-particle measurement to obtain v_n.

Eq. (6) represents the factorization of $V_{n\Delta}(p_T^t, p_T^a)$ into the event-averaged product $\langle v_n\{2\}(p_T^t)\ v_n\{2\}(p_T^a)\rangle$, which includes event-by-event fluctuations. Consistency with Eq. (6) suggests that a large fraction of the particle pairs are correlated through their individual correlation with a common plane of symmetry. For example, symmetry planes for particle pairs at p_T^t and p_T^a may develop at a harmonic order n from collision geometry, initial state density fluctuations, or from an axis formed by (di-)jet fragmentation. If a single-valued $v_n(p_T)$ curve on an interval containing p_T^t and p_T^a can reproduce the magnitude of any $V_{n\Delta}(p_T^t, p_T^a)$, then $V_{n\Delta}$ factorizes within the (p_T^t, p_T^a) region.

Eq. (6) is tested by applying a global fit to the $V_{n\Delta}$ data points over all p_T^t and p_T^a bins simultaneously. This is done separately at each order in n and for each centrality class. An example from the 0–10% most central event class is shown in Fig. 5, where the $V_{n\Delta}$ points for $n = 2$ to 5 are plotted (in separate panels) on a single p_T^t, p_T^a axis as indicated. The global fit function depends on a set of N unconstrained and independent parameters, where N is the number of p_T^t (or p_T^a) bins. The parameters are $v_n\{GF\}(p_T)$, with the fit generating the product $v_n\{GF\}(p_T^t) \times v_n\{GF\}(p_T^a)$ that minimizes the total χ^2 for all $V_{n\Delta}$ points.

The sources of systematic uncertainty of $V_{n\Delta}$ are those that cause $\Delta\phi$-dependent variation on $C(\Delta\phi)$. Factors affecting overall yields such as single-particle inefficiency cancel in the ratio of Eq. (4), and do not generate uncertainty in $C(\Delta\phi)$. Table 1 shows the different contributions to the systematic uncertainty of $V_{n\Delta}$, and Table 2 lists typical magnitudes of these uncertainties for a few representative centrality classes.

The event mixing uncertainty (denoted as "a" in Table 1) accounts for biases due to imperfect matching of event multiplicity and collision vertex position, as well as for finite mixed-event statistics. This uncertainty changes with p_T^t, p_T^a, and centrality. It is evaluated by comparing the $n \leqslant 5$ Fourier sum from $C(\Delta\phi)$ with that from $N_{\text{same}}(\Delta\phi)$. The uncertainty from (a) is depicted by grey bars on the points in $C(\Delta\phi)$ in Fig. 2 and Fig. 3. Due to fluctuations in the mixed-event distribution, uncertainty (a) tends to scale with the $V_{n\Delta}$ statistical error, as shown in the table.

The remainder of the systematic uncertainties are not assigned to $C(\Delta\phi)$, but rather to each $V_{n\Delta}$ directly, where their influence on $V_{n\Delta}$ is more clearly defined. The uncertainty from centrality determination (b) accounts for the resolution and efficiency of the detector used for multiplicity measurements, as well as any biases related to its η acceptance. This uncertainty is globally correlated in centrality. It was studied by conducting the full analysis with the SPD as an alternative centrality estimator, since it has different systematic uncertainties and covers a different pseudorapidity range than the VZERO detectors. The results were found to agree within 1%.

Uncertainty from tracking and momentum resolution (c) was evaluated on $C(\Delta\phi)$ using different track selection criteria. Slightly larger correlation strength is obtained for more restrictive track selection (at the expense of statistical loss), and the difference was found to grow with p_T^a by roughly 1% per GeV/c.

Additional uncertainty is introduced by (d) the finite $\Delta\phi$ bin width, which was estimated by comparing the RMS bin width to the nth harmonic scale, and (e) the precision of the extraction (Eq. (5)). The latter was estimated by calculating $\langle\sin(n\Delta\phi)\rangle$, which is independent of n, and should vanish by symmetry. The residual finite values are used to gauge the corresponding $V_{n\Delta}$ uncertainty. Because the amplitude of the $V_{n\Delta}$ harmonics tends to diminish with increasing n, both uncertainties (d) and (e) are small for $n < 6$ but become comparable to $V_{n\Delta}$ at higher n. Effects (a)–(e) are all combined in quadrature to produce the $V_{n\Delta}$ systematic uncertainties, which are depicted as the solid colored bars on the points in Fig. 4 and Fig. 5. Finally, the uncertainty (f) is included in the quadrature sum with (a)–(e) for $V_{1\Delta}$ only.
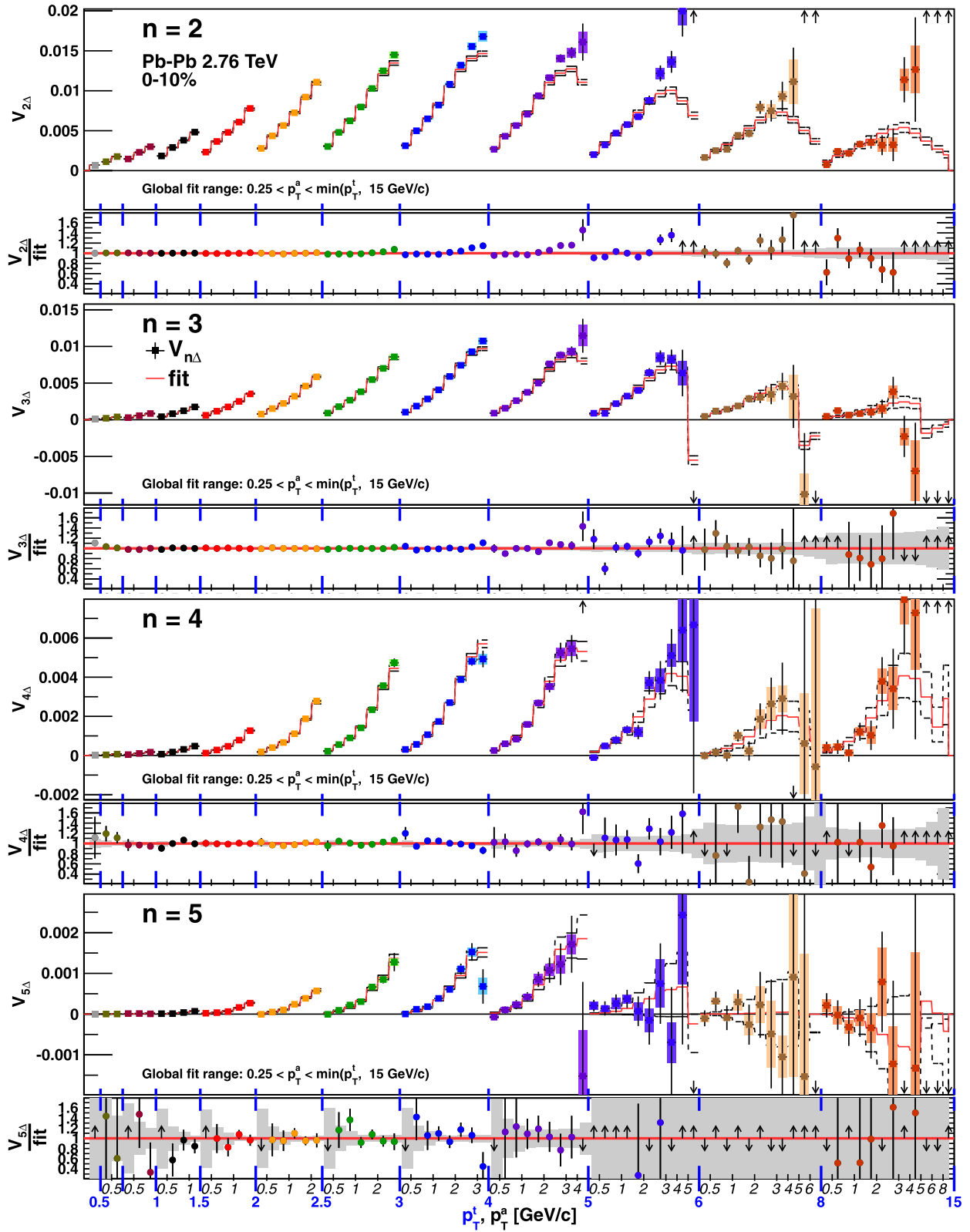
Table 1
Systematic uncertainties on $V_{n\Delta}$.

Contribution	Magnitude
(a) Event mixing	20–30% σ_{stat}
(b) Centrality determination	1% $V_{n\Delta}$
(c) Track selection, p_T resolution	1% $V_{n\Delta} \times \langle p_T^a \rangle$
(d) $\Delta\phi$ bin width	$(0.8n)\%\ V_{n\Delta}$
(e) $V_{n\Delta}$ extraction	<10% $V_{n\Delta}$ ($n < 6$); 10–30% $V_{n\Delta}$ ($n \geqslant 6$)
(f) $V_{n\Delta}$ ($n = 1$ only)	10% $V_{n\Delta} \times \langle p_T^t \rangle\langle p_T^a \rangle$

Table 2
Typical values of $V_{n\Delta}$ systematic uncertainties.

n	Centrality	$\langle V_{n\Delta} \rangle$ ($\times 10^{-3}$)	$\langle \sigma_{\text{sys(tot)}} \rangle$ ($\times 10^{-3}$)	σ_a	σ_b	σ_c ($\times 10^{-3}$)	σ_d	σ_e	σ_f
1	0–10%	4.2	13	0.57	0.042	0.042	0.033	13	0.42
1	20–30%	11	3.7	0.6	0.11	0.11	0.089	3.5	1.1
1	40–50%	23	2.3	0.38	0.23	0.23	0.18	0.31	2.3
2	0–10%	12	7	0.23	0.12	0.12	0.19	7	0
2	20–30%	31	1	0.46	0.31	0.31	0.5	0.6	0
2	40–50%	43	6.9	0.4	0.43	0.43	0.69	6.8	0
3	0–10%	0.82	18	0.29	0.0082	0.0082	0.02	18	0
3	20–30%	2.1	1.4	0.42	0.021	0.021	0.05	1.4	0
3	40–50%	10	4.2	0.42	0.1	0.1	0.25	4.2	0
4	0–10%	2.6	5.4	0.44	0.026	0.026	0.083	5.4	0
4	20–30%	7.2	0.45	0.27	0.072	0.072	0.23	0.26	0
4	40–50%	11	2.6	0.47	0.11	0.11	0.35	2.6	0
5	0–10%	2.6	6.2	0.32	0.026	0.026	0.1	6.1	0
5	20–30%	2.8	3.2	0.17	0.028	0.028	0.11	3.2	0
5	40–50%	6.8	0.6	0.28	0.068	0.068	0.27	0.45	0

Fig. 5. (Color online.) Global fit examples in 0–10% central events for $n = 2, 3, 4$ and 5. The measured $V_{n\Delta}$ coefficients are plotted on an interleaved p_T^t, p_T^a axis in the upper panels, and the global fit function (Eq. (6)) is shown as the red curves. The global fit systematic uncertainty is represented by dashed lines. The lower section of each panel shows the ratio of the data to the fit, and the shaded bands represent the systematic uncertainty propagated to the ratio. In all cases, off-scale points are indicated with arrows.

Fig. 6. (Color online.) The global-fit parameters, $v_n\{GF\}$, for $2 \leqslant n \leqslant 5$. Statistical uncertainties are represented by error bars on the points, while systematic uncertainty is depicted by open rectangles.

Fig. 7. (Color online.) High-p_T fit examples in 0–20% central events for $n = 1$ to 4. Although all datapoints are shown for $p_T^t > 5$ GeV/c, the fit range includes only the six points with $p_T^a > 5$ GeV/c.

To evaluate the systematic uncertainty, the global fit procedure is performed three times for each n and centrality bin: once on the measured $V_{n\Delta}$ points (leading to the red curves in Fig. 5), and once on the upper and lower bounds of the systematic error bars (resulting in black dashed curves). The $v_n\{GF\}$ systematic error is then assigned as half the difference. The resulting uncertainties are shown as open boxes in Fig. 6 and Fig. 11, which are discussed in the following sections.

5. Global fit results

In the $n = 2$ case (Fig. 5, top), the fit agrees well with the data points at low p_T^t and p_T^a, but diverges with increasing p_T^a for each p_T^t interval. Where disagreement occurs, the fit is systematically lower than the points. In contrast, for $n = 3$, the fit does not follow the points that drop sharply to negative values at the highest

momenta. This is also observed for $n = 5$, though with poorer statistical precision.

The global fit is driven primarily by lower particle p_T, where the smaller statistical uncertainties provide a stronger constraint for χ^2 minimization. The disagreement between data and the fit, where p_T^t and p_T^a are both large, points to the breakdown of the factorization hypothesis; see also Fig. 3 and the accompanying discussion.

The factorization hypothesis appears to hold for $n \geqslant 2$ at low p_T^a ($\lesssim 2$ GeV/c) even for the highest p_T^t bins. The $V_{n\Delta}$ values for these cases are small relative to those measured at higher p_T^a, and remain constant or even decrease in magnitude as p_T^t is increased above 3–4 GeV/c. $V_{2\Delta}$ dominates over the other coefficients, and the $n > 3$ terms are not significantly greater than zero. This stands in contrast to the high-p_T^t, high-p_T^a case, where it was demonstrated in Fig. 3 that dijet correlations require signif-
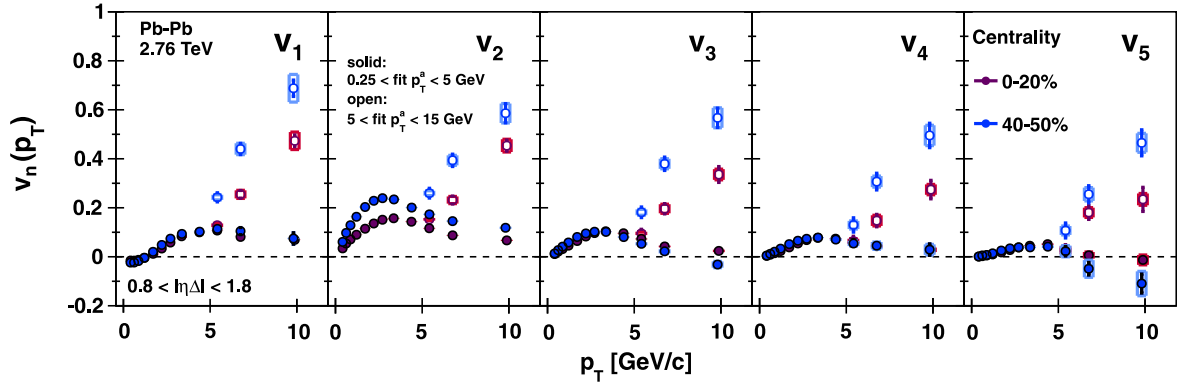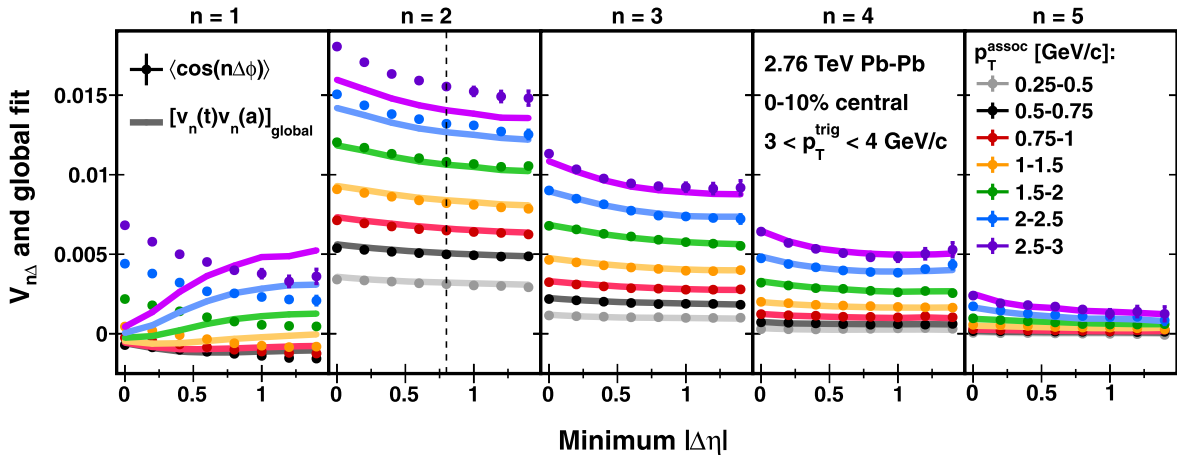
Fig. 8. (Color online.) The global-fit parameters, $v_n\{GF\}$, for $1 \leqslant n \leqslant 5$ as obtained using restricted p_T^a fit ranges at two different centralities. The solid (open) points represent fits using only $0.25 < p_T^a < 5$ ($5 < p_T^a < 15$) GeV/c. The open points represent the magnitude of $v_n\{GF\}$ from high-p_T^t, high-p_T^a long-range correlations. Statistical uncertainties are represented by error bars on the points, while systematic uncertainty is depicted by open rectangles.

Fig. 9. (Color online.) $V_{n\Delta}$ values from 0–10% central Pb–Pb collisions (points) and global fit results (solid lines) for $3.0 < p_T^t < 4.0$ GeV/c as a function of the minimum $|\Delta\eta|$ separation for a selection of p_T^a bins. For clarity, points are shown with statistical error bars only. For reference, a dashed line (drawn only in the $n = 2$ panel) indicates the $|\Delta\eta|_{\min} = 0.8$ requirement applied throughout this analysis.

icant high-order Fourier harmonics to describe the narrow recoil jet peak.

The parameters of the global fit are the best-fit $v_n\{GF\}$ values as a function of p_T, which can be interpreted as the coefficients of Eq. (1). The results of the global fit for $2 \leqslant n \leqslant 5$, denoted $v_n\{GF\}$, are shown in Fig. 6 for several centrality selections. We note that the global fit converges to either positive or negative $v_n\{GF\}$ parameters, depending on the starting point of the fitting routine. The two solutions are equal in magnitude and goodness-of-fit. The positive curves are chosen by convention as shown in Fig. 6. In the 0–2% most central data, $v_3\{GF\}$ ($v_4\{GF\}$) rises with p_T relative to $v_2\{GF\}$ and in fact becomes larger than $v_2\{GF\}$ at approximately 1.5 (2.5) GeV/c. $v_2\{GF\}$ reaches a maximum value near 2.5 GeV/c, whereas the higher harmonics peak at higher p_T. These data are in good agreement with recent two-particle anisotropic flow measurements [31] at the same collision energy, which included a pseudorapidity gap of $|\Delta\eta| > 1.0$.

For $2 \leqslant n \leqslant 5$, the results are not strongly sensitive to the upper p_T^a limit included in the global fit. The global fit was performed not only over the full momentum range (as shown in Fig. 6), but also with the restriction to $V_{n\Delta}$ points with $p_T^a < 2.5$ GeV/c. The outcome was found to be identical to the full fit within one standard deviation. This again reflects the weighting by the steeply-falling particle momentum distribution, indicating that a relatively small number of energetic particles does not strongly bias the event anisotropy, as calculated by the global fit.

If the global fit is applied to $V_{n\Delta}$ points exclusively at large particle momenta, factorization behavior can be tested for correlations that are predominantly jet-induced. An example is shown in Fig. 7, where the global fit has been applied to $V_{n\Delta}$ points within $5 < p_T^a < 15$ GeV/c. In this case, there are six $V_{n\Delta}$ datapoints fitted, and three fit parameters, which are $v_n\{GF\}$ at 5–6, 6–8, and 8–15 GeV/c. An approximate factorization is observed over this range. The agreement between fit and data for the lowest fitted datapoint (at 5–6 GeV/c) is rather poor, indicating that the correlations there are in a transitional region that is less jet-dominated than at higher p_T.

The parameters from the high-p_T global fit can be plotted, just as was done in Fig. 6, to demonstrate their p_T and centrality dependence. However, the sign definition of v_n becomes problematic in the case where $v_n(p_T^t)$ and $v_n(p_T^a)$ have the same sign, but $V_{n\Delta} < 0$. In this case, the v_n coefficients are represented to be positive as a matter of convention.

The fit results from these high-p_T^t, high-p_T^a long-range correlations are shown as open points in Fig. 8. The clear deviation between the two different sets of points demonstrates that it is not possible for a single-valued set of $v_n(p_T)$ points to simultaneously describe both low-p_T^a and high-p_T^a pair anisotropy.

It is instructive to study the dependence of the $V_{n\Delta}$ values on the minimum $|\Delta\eta|$ separation in order to observe the influence of the near-side peak. This is shown in Fig. 9. The $V_{n\Delta}$ values rise as the pseudorapidity gap is reduced and a larger portion of the
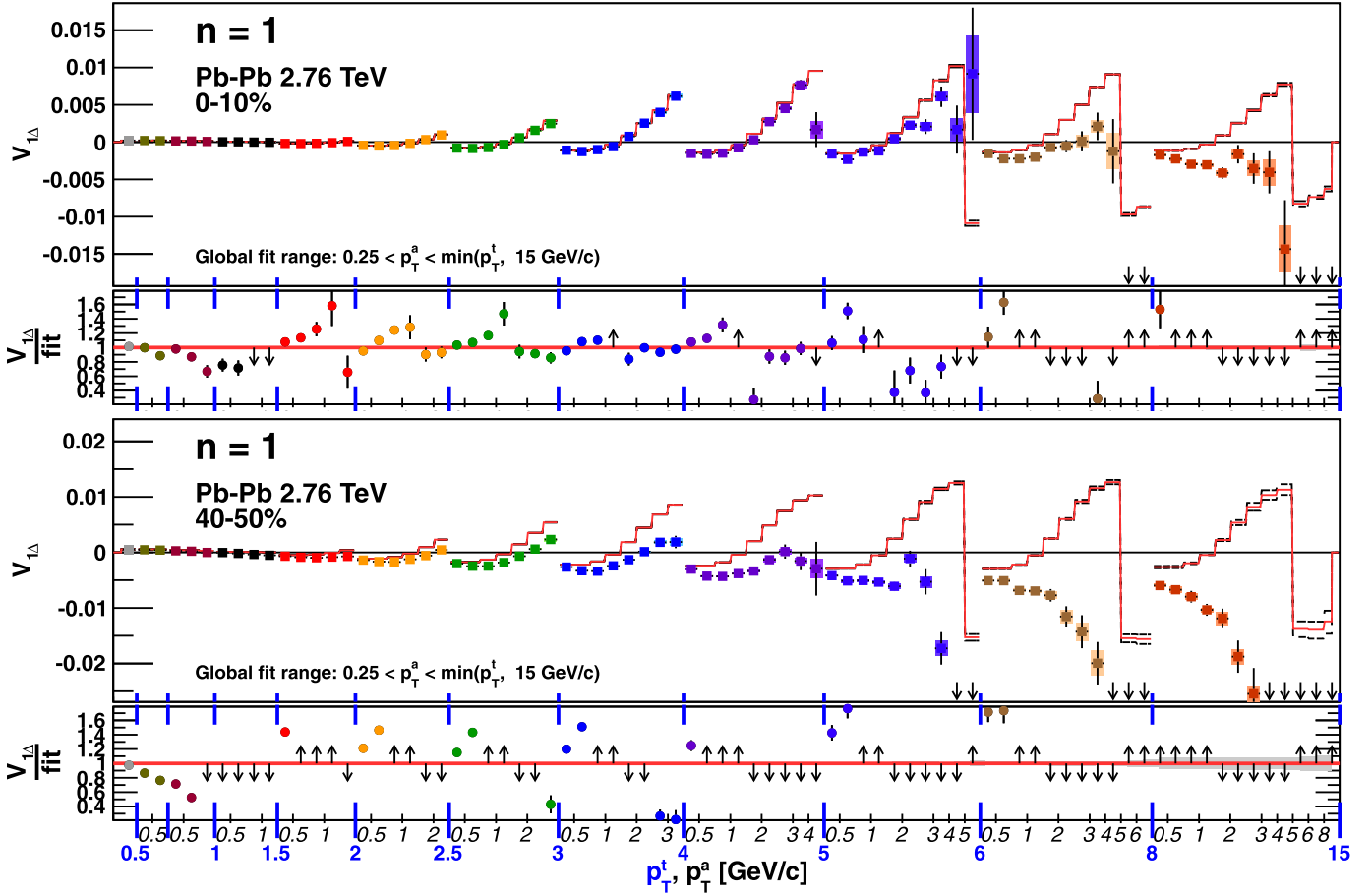
Fig. 10. (Color online.) Global fit examples in 0–10% central (top) and 40–50% central events (bottom) for $n = 1$. The uncertainties are represented in the same way as for Fig. 5.
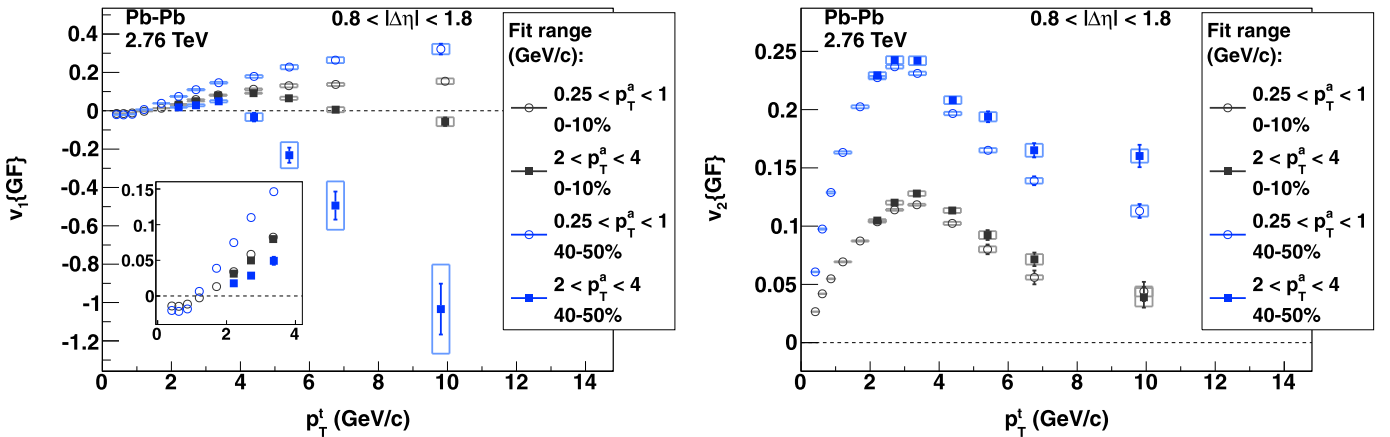

Fig. 11. (Color online.) $v_1\{GF\}$ (left) and $v_2\{GF\}$ (right) as obtained using restricted p_T^a fit ranges at two different centralities. The open circles (solid squares) represent fits using only $0.25 < p_T^a < 1$ ($2 < p_T^a < 4$) GeV/c. For the more central v_2 points, the two different fit ranges lead to a similar curve, indicating an approximate factorization. In contrast, a divergence with rising p_T^t is observed for $v_1\{GF\}$. For both $n = 1$ and $n = 2$, the divergence is enhanced in more peripheral centrality classes.

near-side peak is included in the correlations. At $p_T^t > 3$–4 GeV/c, the peak is narrow and the curves are fairly flat at $|\Delta\eta| > 0.5$. For the 3–4 GeV/c range shown in the figure, there is a discernible contribution from the near-side peak, but the difference does not exceed a few percent at $|\Delta\eta| > 0.8$.

For the first harmonic, the disagreement grows significantly as $|\Delta\eta|$ is decreased, while the higher harmonics exhibit a much lower sensitivity to $|\Delta\eta|_{min}$. Even if a large η gap is applied, how-

ever, Fig. 9 indicates that an accurate global description of $V_{1\Delta}$ is still not obtained, even at these low to intermediate p_T values.

This behavior is representative of a general lack of consistent $V_{1\Delta}$ factorization, as demonstrated in Fig. 10 where the global fit for $n = 1$ is shown for two centrality ranges. However, a reasonable fit is obtained if the p_T^a range is restricted to smaller intervals. Fig. 11 shows the result of performing the global fit to v_1 (left) and v_2 (right) over $0.25 < p_T^a < 1.0$ and $2 < p_T^a < 4$ GeV/c

separately at two different centralities. In the case of v_1, a divergence occurs between the results obtained from the two different p_T^a bins, which is more prominent in mid-central collisions. For 0–20% v_2, however, fits using the two different p_T^a intervals lead to approximately the same curve, supporting the observation that v_2 factorizes: on average over events in this centrality category, a unique symmetry plane exists for the majority of all particles below 4 GeV/c. The systematic increase of the higher p_T^a fit compared to $p_T^a < 1$ is likely from nonflow contributions on the away side, which are larger in the more peripheral centralities because of reduced quenching effects. Thus the observed patterns follow the expected trends with p_T^a and centrality.

The breakdown of factorization for $V_{1\Delta}$ does not imply that there is no real collective v_1 since the collective part may not be the dominant contribution to $V_{1\Delta}$. It is therefore interesting to note that at low p_T, the best-fit $v_1\{GF\}$ values become negative, as observed in hydrodynamic simulations with fluctuating initial conditions [43]. Although those calculations were for Au + Au collisions at 200 GeV, qualitatively similar results have been obtained at 2.76 TeV [44]. Estimation of the effect of momentum conservation as a correction to the coefficients prior to the global fit is currently under investigation. In [43], such a correction amounted to a change in v_1 of about 0.01–0.02. In this analysis we have included a systematic uncertainty of 10% $\langle p_T^a \rangle$ in $V_{1\Delta}$ to account for the bias resulting from the neglect of this correction, and the uncertainty is propagated to $v_1\{GF\}$ in the same fashion as for $n > 1$. Further studies will be required to unambiguously extract the collective part of $V_{1\Delta}$.

6. Summary

The shape evolution of triggered pair distributions was investigated quantitatively using a discrete Fourier decomposition. In the bulk-dominated p_T regime, a distinct near-side ridge and a doubly-peaked away-side structure are observed in the most central events, both persisting to a large relative pseudorapidity interval between trigger and associated particles. These features are represented in Fourier spectra by harmonic amplitudes, both even and odd, which are finite in magnitude up to approximately $n = 5$. These pair anisotropies are found to approximately factorize into single-particle harmonic coefficients for $p_T^a < 4$ GeV/c, with the notable exception of $V_{1\Delta}$. This factorization is consistent with expectations from collective response to anisotropic initial conditions, which provides a complete and self-consistent picture explaining the observed features without invocation of dynamical mechanisms such as Mach shock waves [45].

The data also suggest that at low p_T (below approximately 3 GeV/c), any contribution from the away-side jet is constrained to be relatively small. In contrast, for associated p_T greater than 4–6 GeV/c, the long-range correlation appears dominated by a large peak from the recoil jet. In this regime, when both particles are at high momenta, the anisotropy does not follow the p_T-dependent pattern followed by particle pairs at lower p_T^a. The global fit technique provides a means of identifying transitions in the momentum and centrality dependence of correlations with respect to symmetry planes. Within the bulk-dominated region, the measurement of all significant harmonics provides the possibility to constrain the geometry of the fluctuating initial state and further understand the nuclear medium through its collective response.

Acknowledgements

Open access

References

[1] I. Arsene, et al., Nucl. Phys. A 757 (2005) 1.
[2] B.B. Back, et al., Nucl. Phys. A 757 (2005) 28.
[3] J. Adams, et al., Nucl. Phys. A 757 (2005) 102.
[4] K. Adcox, et al., Nucl. Phys. A 757 (2005) 184.
[5] K. Aamodt, et al., Phys. Rev. Lett. 105 (2010) 252302.
[6] ATLAS Collaboration, Measurement of the pseudorapidity and transverse momentum dependence of the elliptic flow of charged particles in lead–lead collisions at $\sqrt{s_{NN}} = 2.76$ TeV with the ATLAS detector, arXiv:1108.6018 [hep-ex], 2011.
[7] C. Adler, et al., Phys. Rev. Lett. 90 (2003) 082302.
[8] J. Adams, et al., Phys. Rev. Lett. 95 (2005) 152301.
[9] A. Adare, et al., Phys. Rev. Lett. 98 (2007) 232302.
[10] J. Adams, et al., Phys. Rev. Lett. 97 (2006) 162301.
[11] B. Alver, et al., Phys. Rev. C 81 (2010) 024904.
[12] A. Adare, et al., Phys. Rev. C 78 (2008) 014901.
[13] B.I. Abelev, et al., Phys. Rev. C 80 (2009) 064912.
[14] B. Alver, et al., Phys. Rev. Lett. 104 (2010) 062301.
[15] A. Adare, et al., Phys. Rev. Lett. 104 (2010) 252301.
[16] V. Khachatryan, et al., JHEP 1009 (2010) 091.
[17] C. Aad, et al. Measurement of elliptic flow and higher-order flow coefficients with the ATLAS detector in $\sqrt{s_{NN}} = 2.76$ TeV Pb + Pb collisions, Technical Report ATLAS-CONF-2011-074, CERN, Geneva, 2011.
[18] S. Chatrchyan, et al., Long-range and short-range dihadron angular correlations in central PbPb collisions at a nucleon–nucleon center of mass energy of 2.76 TeV, arXiv:1105.2438 [nucl-ex], 2011.
[19] S. Voloshin, Phys. Lett. B 632 (2006) 490.
[20] N. Armesto, C.A. Salgado, U.A. Wiedemann, Phys. Rev. Lett. 93 (2004) 242301.
[21] C.B. Chiu, R.C. Hwa, Phys. Rev. C 72 (2005) 034903.
[22] P. Romatschke, Phys. Rev. C 75 (2007) 014901.
[23] A. Majumder, B. Muller, S.A. Bass, Phys. Rev. Lett. 99 (2007) 042301.
[24] E.V. Shuryak, Phys. Rev. C 76 (2007) 047901.
[25] C.-Y. Wong, Phys. Rev. C 78 (2008) 064905.
[26] A. Dumitru, F. Gelis, L. McLerran, R. Venugopalan, Nucl. Phys. A 810 (2008) 91.
[27] S. Gavin, L. McLerran, G. Moschelli, Phys. Rev. C 79 (2009) 051902.
[28] K. Dusling, D. Fernandez-Fraile, R. Venugopalan, Nucl. Phys. A 828 (2009) 161.
[29] Y. Hama, R.P.G. Andrade, F. Grassi, W.-L. Qian, Nonlin. Phenom. Complex Syst. 12 (2009) 466.
[30] A. Morsch, On the mean parton transverse momentum versus associated hadron $p(T)$ in di-hadron correlations at RHIC and LHC, arXiv:hep-ph/0606098, 2006.
[31] K. Aamodt, et al., Phys. Rev. Lett. 107 (2011) 032301.
[32] S. Manly, et al., Nucl. Phys. A 774 (2006) 523.
[33] B. Alver, et al., Phys. Rev. Lett. 98 (2007) 242302.
[34] A.P. Mishra, R.K. Mohapatra, P.S. Saumia, A.M. Srivastava, Phys. Rev. C 77 (2008) 064902.
[35] A.P. Mishra, R.K. Mohapatra, P.S. Saumia, A.M. Srivastava, Phys. Rev. C 81 (2010) 034903.
[36] J. Takahashi, et al., Phys. Rev. Lett. 103 (2009) 242301.
[37] P. Sorensen, J. Phys. G: Nucl. Part. Phys. 37 (2010) 094011.
[38] B. Alver, G. Roland, Phys. Rev. C 81 (2010) 054905.
[39] D. Teaney, L. Yan, Triangularity and dipole asymmetry in heavy ion collisions, arXiv:1010.1876 [nucl-th], 2010.
[40] M. Luzum, Phys. Lett. B 696 (2011) 499.
[41] A. Adare, et al., Measurements of higher-order flow harmonics in Au + Au collisions at $\sqrt{s_{NN}} = 200$ GeV, arXiv:1105.3928 [nucl-ex], 2011.
[42] K. Aamodt, et al., Phys. Rev. Lett. 106 (2011) 032301.
[43] F.G. Gardim, F. Grassi, Y. Hama, M. Luzum, J.-Y. Ollitrault, Phys. Rev. C 83 (2011) 064901.
[44] M. Luzum, private communication, 2011.
[45] J. Casalderrey-Solana, E.V. Shuryak, D. Teaney, Nucl. Phys. A 774 (2006) 577.

ALICE Collaboration

K. Aamodt [a], B. Abelev [b], A. Abrahantes Quintana [c], D. Adamová [d], A.M. Adare [e,*], M.M. Aggarwal [f], G. Aglieri Rinella [g], A.G. Agocs [h], A. Agostinelli [i], S. Aguilar Salazar [j], Z. Ahammed [k], N. Ahmad [l], A. Ahmad Masoodi [l], S.U. Ahn [m,1], A. Akindinov [n], D. Aleksandrov [o], B. Alessandro [p], R. Alfaro Molina [j], A. Alici [q,2], A. Alkin [r], E. Almaráz Aviña [j], J. Alme [s], T. Alt [t], V. Altini [u], S. Altinpinar [a], I. Altsybeev [v], C. Andrei [w], A. Andronic [x], V. Anguelov [t,3], J. Anielski [y], T. Antičić [z], F. Antinori [aa], P. Antonioli [ab], L. Aphecetche [ac], H. Appelshäuser [ad], N. Arbor [ae], S. Arcelli [i], A. Arend [ad], N. Armesto [af], R. Arnaldi [p], T. Aronsson [e], I.C. Arsene [x], M. Arslandok [ad], A. Asryan [v], A. Augustinus [g], R. Averbeck [x], T.C. Awes [ag], J. Äystö [ah], M.D. Azmi [l], M. Bach [t], A. Badalà [ai], Y.W. Baek [m,4], R. Bailhache [ad], R. Bala [p], R. Baldini Ferroli [q], A. Baldisseri [aj], A. Baldit [ak], F. Baltasar Dos Santos Pedrosa [g], J. Bán [al], R.C. Baral [am], R. Barbera [an], F. Barile [u], G.G. Barnaföldi [h], L.S. Barnby [ao], V. Barret [ak], J. Bartke [ap], M. Basile [i], N. Bastid [ak], B. Bathen [y], G. Batigne [ac], B. Batyunya [aq], C. Baumann [ad], I.G. Bearden [ar], H. Beck [ad], I. Belikov [as], F. Bellini [i], R. Bellwied [at], E. Belmont-Moreno [j], S. Beole [au], I. Berceanu [w], A. Bercuci [w], Y. Berdnikov [av], D. Berenyi [h], C. Bergmann [y], L. Betev [g], A. Bhasin [aw], A.K. Bhati [f], L. Bianchi [au], N. Bianchi [ax], C. Bianchin [ay], J. Bielčík [az], J. Bielčíková [d], A. Bilandzic [ba], E. Biolcati [au], F. Blanco [bb], F. Blanco [at], D. Blau [o], C. Blume [ad], N. Bock [bc], A. Bogdanov [bd], H. Bøggild [ar], M. Bogolyubsky [be], L. Boldizsár [h], M. Bombara [bf], C. Bombonati [ay], J. Book [ad], H. Borel [aj], A. Borissov [bg], C. Bortolin [ay,5], S. Bose [bh], F. Bossú [au], M. Botje [ba], S. Böttger [bi], B. Boyer [bj], P. Braun-Munzinger [x], M. Bregant [ac], T. Breitner [bi], M. Broz [bk], R. Brun [g], E. Bruna [e,6], G.E. Bruno [u], D. Budnikov [bl], H. Buesching [ad], S. Bufalino [p], K. Bugaiev [r], O. Busch [bm], Z. Buthelezi [bn], D. Caffarri [ay], X. Cai [bo], H. Caines [e], E. Calvo Villar [bp], P. Camerini [bq], V. Canoa Roman [br,7], G. Cara Romeo [ab], F. Carena [g], W. Carena [g], F. Carminati [g], A. Casanova Díaz [ax], M. Caselle [g], J. Castillo Castellanos [aj], E.A.R. Casula [bs], V. Catanescu [w], C. Cavicchioli [g], J. Cepila [az], P. Cerello [p], B. Chang [ah], S. Chapeland [g], J.L. Charvet [aj], S. Chattopadhyay [bh], S. Chattopadhyay [k], M. Cherney [bt], C. Cheshkov [bu], B. Cheynis [bu], E. Chiavassa [p], V. Chibante Barroso [g], D.D. Chinellato [bv], P. Chochula [g], M. Chojnacki [bw], P. Christakoglou [bw], C.H. Christensen [ar], P. Christiansen [bx], T. Chujo [by], S.U. Chung [bz], C. Cicalo [ca], L. Cifarelli [i,8], F. Cindolo [ab], J. Cleymans [bn], F. Coccetti [q], J.-P. Coffin [as], F. Colamaria [u], D. Colella [u], G. Conesa Balbastre [ae], Z. Conesa del Valle [as,9], P. Constantin [bm], G. Contin [bq], J.G. Contreras [br], T.M. Cormier [bg], Y. Corrales Morales [au], I. Cortés Maldonado [cb], P. Cortese [cc], M.R. Cosentino [bv,10], F. Costa [g], M.E. Cotallo [bb],

P. Crochet [ak], E. Cruz Alaniz [j], E. Cuautle [cd], L. Cunqueiro [ax], G.D. Erasmo [u], A. Dainese [aa], H.H. Dalsgaard [ar], A. Danu [ce], D. Das [bh], I. Das [bh], K. Das [bh], A. Dash [bv], S. Dash [p], S. De [k], A. De Azevedo Moregula [ax], G.O.V. de Barros [cf], A. De Caro [cg,11], G. de Cataldo [ch], J. de Cuveland [t], A. De Falco [bs], D. De Gruttola [cg], N. De Marco [p], S. De Pasquale [cg], R. de Rooij [bw], E. Del Castillo Sanchez [g], H. Delagrange [ac], A. Deloff [ci], V. Demanov [bl], E. Dénes [h], A. Deppman [cf], D. Di Bari [u], C. Di Giglio [u], S. Di Liberto [cj], A. Di Mauro [g], P. Di Nezza [ax], T. Dietel [y], R. Divià [g], Ø. Djuvsland [a], A. Dobrin [bg], T. Dobrowolski [ci], I. Domínguez [cd], B. Dönigus [x], O. Dordic [ck], O. Driga [ac], A.K. Dubey [k], L. Ducroux [bu], P. Dupieux [ak], A.K. Dutta Majumdar [bh], M.R. Dutta Majumdar [k], D. Elia [ch], D. Emschermann [y], H. Engel [bi], H.A. Erdal [s], B. Espagnon [bj], M. Estienne [ac], S. Esumi [by], D. Evans [ao], G. Eyyubova [ck], D. Fabris [aa], J. Faivre [ae], D. Falchieri [i], A. Fantoni [ax], M. Fasel [x], R. Fearick [bn], A. Fedunov [aq], D. Fehlker [a], D. Felea [ce], B. Fenton-Olsen [cl], G. Feofilov [v], A. Fernández Téllez [cb], E.G. Ferreiro [af], A. Ferretti [au], R. Ferretti [cc], J. Figiel [ap], M.A.S. Figueredo [cf], S. Filchagin [bl], R. Fini [ch], D. Finogeev [cm], F.M. Fionda [u], E.M. Fiore [u], M. Floris [g], S. Foertsch [bn], P. Foka [x], S. Fokin [o], E. Fragiacomo [cn], M. Fragkiadakis [co], U. Frankenfeld [x], U. Fuchs [g], C. Furget [ae], M. Fusco Girard [cg], J.J. Gaardhøje [ar], M. Gagliardi [au], A. Gago [bp], M. Gallio [au], D.R. Gangadharan [bc], P. Ganoti [ag], C. Garabatos [x], E. Garcia-Solis [cp], I. Garishvili [b], J. Gerhard [t], M. Germain [ac], C. Geuna [aj], A. Gheata [g], M. Gheata [g], B. Ghidini [u], P. Ghosh [k], P. Gianotti [ax], M.R. Girard [cq], P. Giubellino [au,9], E. Gladysz-Dziadus [ap], P. Glässel [bm], R. Gomez [cr], L.H. González-Trueba [j], P. González-Zamora [bb], S. Gorbunov [t], A. Goswami [cs], S. Gotovac [ct], V. Grabski [j], L.K. Graczykowski [cq], R. Grajcarek [bm], A. Grelli [bw], A. Grigoras [g], C. Grigoras [g], V. Grigoriev [bd], A. Grigoryan [cu], S. Grigoryan [aq], B. Grinyov [r], N. Grion [cn], J.F. Grosse-Oetringhaus [g], J.-Y. Grossiord [bu], F. Guber [cm], R. Guernane [ae], C. Guerra Gutierrez [bp], B. Guerzoni [i], M. Guilbaud [bu], K. Gulbrandsen [ar], T. Gunji [cv], A. Gupta [aw], R. Gupta [aw], H. Gutbrod [x], Ø. Haaland [a], C. Hadjidakis [bj], M. Haiduc [ce], H. Hamagaki [cv], G. Hamar [h], L.D. Hanratty [ao], Z. Harmanova [bf], J.W. Harris [e], M. Hartig [ad], D. Hasegan [ce], D. Hatzifotiadou [ab], A. Hayrapetyan [cu,8], M. Heide [y], H. Helstrup [s], A. Herghelegiu [w], G. Herrera Corral [br], N. Herrmann [bm], K.F. Hetland [s], B. Hicks [e], P.T. Hille [e], B. Hippolyte [as], T. Horaguchi [by], Y. Hori [cv], P. Hristov [g], I. Hřivnáčová [bj], M. Huang [a], S. Huber [x], T.J. Humanic [bc], D.S. Hwang [cw], R. Ichou [ak], R. Ilkaev [bl], I. Ilkiv [ci], M. Inaba [by], E. Incani [bs], G.M. Innocenti [au], M. Ippolitov [o], M. Irfan [l], C. Ivan [x], A. Ivanov [v], M. Ivanov [x], V. Ivanov [av], O. Ivanytskyi [r], P.M. Jacobs [cl], L. Jancurová [aq], S. Jangal [as], M.A. Janik [cq], R. Janik [bk], P.H.S.Y. Jayarathna [at], S. Jena [cx], R.T. Jimenez Bustamante [cd], L. Jirden [g], P.G. Jones [ao], H. Jung [m], W. Jung [m], A. Jusko [ao], S. Kalcher [t], P. Kaliňák [al], M. Kalisky [y], T. Kalliokoski [ah], A. Kalweit [cy], K. Kanaki [a], J.H. Kang [cz], V. Kaplin [bd], A. Karasu Uysal [g], O. Karavichev [cm], T. Karavicheva [cm], E. Karpechev [cm], A. Kazantsev [o], U. Kebschull [bi], R. Keidel [da], M.M. Khan [l], P. Khan [bh], S.A. Khan [k], A. Khanzadeev [av], Y. Kharlov [be], B. Kileng [s], B. Kim [cz], D.J. Kim [ah], D.W. Kim [m], J.H. Kim [cw], J.S. Kim [m], M. Kim [cz], S. Kim [cw], S.H. Kim [m], T. Kim [cz], S. Kirsch [t], I. Kisel [t], S. Kiselev [n], A. Kisiel [g,12], J.L. Klay [db], J. Klein [bm], C. Klein-Bösing [y], M. Kliemant [ad], A. Kluge [g], M.L. Knichel [x], K. Koch [bm], M.K. Köhler [x], A. Kolojvari [v], V. Kondratiev [v], N. Kondratyeva [bd], A. Konevskikh [cm], C. Kottachchi Kankanamge Don [bg], R. Kour [ao], M. Kowalski [ap], S. Kox [ae], G. Koyithatta Meethaleveedu [cx], J. Kral [ah], I. Králik [al], F. Kramer [ad], I. Kraus [x], T. Krawutschke [bm,13], M. Kretz [t], M. Krivda [ao,14], F. Krizek [ah], M. Krus [az], E. Kryshen [av], M. Krzewicki [ba], Y. Kucheriaev [o], C. Kuhn [as], P.G. Kuijer [ba], P. Kurashvili [ci], A. Kurepin [cm], A.B. Kurepin [cm], A. Kuryakin [bl], S. Kushpil [d], V. Kushpil [d], M.J. Kweon [bm], Y. Kwon [cz], P. La Rocca [an], P. Ladrón de Guevara [cd], I. Lakomov [v], C. Lara [bi], A. Lardeux [ac], D.T. Larsen [a], C. Lazzeroni [ao], Y. Le Bornec [bj], R. Lea [bq], M. Lechman [g], K.S. Lee [m], S.C. Lee [m], F. Lefèvre [ac], J. Lehnert [ad], L. Leistam [g], M. Lenhardt [ac], V. Lenti [ch], I. León Monzón [cr], H. León Vargas [ad], P. Lévai [h], X. Li [dc], J. Lien [a], R. Lietava [ao], S. Lindal [ck], V. Lindenstruth [t], C. Lippmann [x], M.A. Lisa [bc], L. Liu [a], P.I. Loenne [a], V.R. Loggins [bg], V. Loginov [bd], S. Lohn [g], D. Lohner [bm], C. Loizides [cl], K.K. Loo [ah], X. Lopez [ak], E. López Torres [c], G. Løvhøiden [ck], X.-G. Lu [bm], P. Luettig [ad], M. Lunardon [ay], J. Luo [bo], G. Luparello [au], L. Luquin [ac], C. Luzzi [g], R. Ma [e], A. Maevskaya [cm], M. Mager [g], D.P. Mahapatra [am], A. Maire [as], M. Malaev [av], I. Maldonado Cervantes [cd], L. Malinina [aq,15], D. Mal'Kevich [n], P. Malzacher [x], A. Mamonov [bl], L. Manceau [p], V. Manko [o], F. Manso [ak], V. Manzari [ch], Y. Mao [bo,16], M. Marchisone [au,1], J. Mareš [dd], G.V. Margagliotti [bq], A. Margotti [ab], A. Marín [x], C. Markert [de], I. Martashvili [df], P. Martinengo [g], M.I. Martínez [cb], A. Martínez Davalos [j], G. Martínez García [ac], Y. Martynov [r], A. Mas [ac], S. Masciocchi [x], M. Masera [au], A. Masoni [ca], L. Massacrier [bu], M. Mastromarco [ch], A. Mastroserio [g,17], Z.L. Matthews [ao], A. Matyja [ap,18], D. Mayani [cd], C. Mayer [ap], M.A. Mazzoni [cj], F. Meddi [dg], A. Menchaca-Rocha [j], J. Mercado Pérez [bm], M. Meres [bk], Y. Miake [by], A. Michalon [as], J. Midori [dh], L. Milano [au], J. Milosevic [ck,19],

A. Mischke [bw], A.N. Mishra [cs], D. Miśkowiec [g], C. Mitu [ce], J. Mlynarz [bg], A.K. Mohanty [g], B. Mohanty [k], L. Molnar [g], L. Montaño Zetina [br], M. Monteno [p], E. Montes [bb], T. Moon [cz], M. Morando [ay], D.A. Moreira De Godoy [cf], S. Moretto [ay], A. Morsch [g], V. Muccifora [ax], E. Mudnic [ct], H. Müller [g], S. Muhuri [k], M.G. Munhoz [cf], L. Musa [g], A. Musso [p], J.L. Nagle [ar], B.K. Nandi [cx], R. Nania [ab], E. Nappi [ch], C. Nattrass [df], N.P. Naumov [bl], S. Navin [ao], T.K. Nayak [k], S. Nazarenko [bl], G. Nazarov [bl], A. Nedosekin [n], M. Nicassio [u], B.S. Nielsen [ar], T. Niida [by], S. Nikolaev [o], V. Nikolic [z], S. Nikulin [o], V. Nikulin [av], B.S. Nilsen [bt], M.S. Nilsson [ck], F. Noferini [q,2], P. Nomokonov [aq], G. Nooren [bw], N. Novitzky [ah], A. Nyanin [o], A. Nyatha [cx], C. Nygaard [ar], J. Nystrand [a], H. Obayashi [dh], A. Ochirov [v], H. Oeschler [cy], S.K. Oh [m], J. Oleniacz [cq], C. Oppedisano [p], A. Ortiz Velasquez [cd], G. Ortona [au], A. Oskarsson [bx], I. Otterlund [bx], J. Otwinowski [x], G. Øvrebekk [a], K. Oyama [bm], Y. Pachmayer [bm], M. Pachr [az], F. Padilla [au], P. Pagano [cg], G. Paić [cd], F. Painke [t], C. Pajares [af], S. Pal [aj], S.K. Pal [k], A. Palaha [ao], A. Palmeri [ai], G.S. Pappalardo [ai], W.J. Park [x], A. Passfeld [y], D.I. Patalakha [be], V. Paticchio [ch], A. Pavlinov [bg], T. Pawlak [cq], T. Peitzmann [bw], E. Pereira De Oliveira Filho [cf], D. Peresunko [o], C.E. Pérez Lara [ba], E. Perez Lezama [cd], D. Perini [g], D. Perrino [u], W. Peryt [cq], A. Pesci [ab], V. Peskov [g,20], Y. Pestov [di], V. Petráček [az], M. Petran [az], M. Petris [w], P. Petrov [ao], M. Petrovici [w], C. Petta [an], S. Piano [cn], A. Piccotti [p], M. Pikna [bk], P. Pillot [ac], O. Pinazza [g], L. Pinsky [at], N. Pitz [ad], F. Piuz [g], D.B. Piyarathna [at], M. Płoskoń [cl], J. Pluta [cq], T. Pocheptsov [aq], S. Pochybova [h], P.L.M. Podesta-Lerma [cr], M.G. Poghosyan [au], B. Polichtchouk [be], A. Pop [w], S. Porteboeuf-Houssais [ak], V. Pospíšil [az], B. Potukuchi [aw], S.K. Prasad [bg], R. Preghenella [q,2], F. Prino [p], C.A. Pruneau [bg], I. Pshenichnov [cm], G. Puddu [bs], A. Pulvirenti [an], V. Punin [bl], M. Putiš [bf], J. Putschke [e,21], E. Quercigh [g], H. Qvigstad [ck], A. Rachevski [cn], A. Rademakers [g], S. Radomski [bm], T.S. Räihä [ah], J. Rak [ah], A. Rakotozafindrabe [aj], L. Ramello [cc], A. Ramírez Reyes [br], R. Raniwala [cs], S. Raniwala [cs], S.S. Räsänen [ah], B.T. Rascanu [ad], D. Rathee [f], K.F. Read [df], J.S. Real [ae], K. Redlich [ci], P. Reichelt [ad], M. Reicher [bw], R. Renfordt [ad], A.R. Reolon [ax], A. Reshetin [cm], F. Rettig [t], J.-P. Revol [g], K. Reygers [bm], H. Ricaud [cy], L. Riccati [p], R.A. Ricci [dj], M. Richter [a,22], P. Riedler [g], W. Riegler [g], F. Riggi [an], M. Rodríguez Cahuantzi [cb], D. Rohr [t], D. Röhrich [a], R. Romita [x], F. Ronchetti [ax], P. Rosnet [ak], S. Rossegger [g], A. Rossi [ay], F. Roukoutakis [co], C. Roy [as], P. Roy [bh], A.J. Rubio Montero [bb], R. Rui [bq], E. Ryabinkin [o], A. Rybicki [ap], S. Sadovsky [be], K. Šafařík [g], P.K. Sahu [am], J. Saini [k], H. Sakaguchi [dh], S. Sakai [cl], D. Sakata [by], C.A. Salgado [af], S. Sambyal [aw], V. Samsonov [av], X. Sanchez Castro [cd], L. Šándor [al], A. Sandoval [j], M. Sano [by], S. Sano [cv], R. Santo [y], R. Santoro [ch,9], J. Sarkamo [ah], E. Scapparone [ab], F. Scarlassara [ay], R.P. Scharenberg [dk], C. Schiaua [w], R. Schicker [bm], C. Schmidt [x], H.R. Schmidt [x,23], S. Schreiner [g], S. Schuchmann [ad], J. Schukraft [g], Y. Schutz [ac,8], K. Schwarz [x], K. Schweda [bm,24], G. Scioli [i], E. Scomparin [p], P.A. Scott [ao], R. Scott [df], G. Segato [ay], I. Selyuzhenkov [x], S. Senyukov [cc,25], S. Serci [bs], E. Serradilla [j,26], A. Sevcenco [ce], I. Sgura [ch], G. Shabratova [aq], R. Shahoyan [g], N. Sharma [f], S. Sharma [aw], K. Shigaki [dh], M. Shimomura [by], K. Shtejer [c], Y. Sibiriak [o], M. Siciliano [au], E. Sicking [g], S. Siddhanta [ca], T. Siemiarczuk [ci], D. Silvermyr [ag], G. Simonetti [g], R. Singaraju [k], R. Singh [aw], S. Singha [k], B.C. Sinha [k], T. Sinha [bh], B. Sitar [bk], M. Sitta [cc], T.B. Skaali [ck], K. Skjerdal [a], R. Smakal [az], N. Smirnov [e], R. Snellings [bw], C. Søgaard [ar], R. Soltz [b], H. Son [cw], J. Song [bz], M. Song [cz], C. Soos [g], F. Soramel [ay], M. Spyropoulou-Stassinaki [co], B.K. Srivastava [dk], J. Stachel [bm], I. Stan [ce], G. Stefanek [ci], G. Stefanini [g], T. Steinbeck [t], M. Steinpreis [bc], E. Stenlund [bx], G. Steyn [bn], D. Stocco [ac], M. Stolpovskiy [be], P. Strmen [bk], A.A.P. Suaide [cf], M.A. Subieta Vásquez [au], T. Sugitate [dh], C. Suire [bj], M. Sukhorukov [bl], R. Sultanov [n], M. Šumbera [d], T. Susa [z], A. Szanto de Toledo [cf], I. Szarka [bk], A. Szostak [a], C. Tagridis [co], J. Takahashi [bv], J.D. Tapia Takaki [bj], A. Tauro [g], G. Tejeda Muñoz [cb], A. Telesca [g], C. Terrevoli [u], J. Thäder [x], D. Thomas [bw], J.H. Thomas [x], R. Tieulent [bu], A.R. Timmins [at], D. Tlusty [az], A. Toia [g], H. Torii [dh,27], F. Tosello [p], T. Traczyk [cq], W.H. Trzaska [ah], T. Tsuji [cv], A. Tumkin [bl], R. Turrisi [aa], A.J. Turvey [bt], T.S. Tveter [ck], J. Ulery [ad], K. Ullaland [a], J. Ulrich [bi], A. Uras [bu], J. Urbán [bf], G.M. Urciuoli [cj], G.L. Usai [bs], M. Vajzer [az,28], M. Vala [aq,14], L. Valencia Palomo [bj], S. Vallero [bm], N. van der Kolk [ba], M. van Leeuwen [bw], P. Vande Vyvre [g], L. Vannucci [dj], A. Vargas [cb], R. Varma [cx], M. Vasileiou [co], A. Vasiliev [o], V. Vechernin [v], M. Veldhoen [bw], M. Venaruzzo [bq], E. Vercellin [au], S. Vergara [cb], D.C. Vernekohl [y], R. Vernet [dl], M. Verweij [bw], L. Vickovic [ct], G. Viesti [ay], O. Vikhlyantsev [bl], Z. Vilakazi [bn], O. Villalobos Baillie [ao], A. Vinogradov [o], L. Vinogradov [v], Y. Vinogradov [bl], T. Virgili [cg], Y.P. Viyogi [k], A. Vodopyanov [aq], K. Voloshin [n], S. Voloshin [bg], G. Volpe [u,9], B. von Haller [g], D. Vranic [x], J. Vrláková [bf], B. Vulpescu [ak], A. Vyushin [bl], B. Wagner [a], V. Wagner [az], R. Wan [as,29], D. Wang [bo], M. Wang [bo], Y. Wang [bm], Y. Wang [bo], K. Watanabe [by], J.P. Wessels [y,9], U. Westerhoff [y], J. Wiechula [bm,23], J. Wikne [ck], M. Wilde [y], A. Wilk [y], G. Wilk [ci], M.C.S. Williams [ab], B. Windelband [bm],

L. Xaplanteris Karampatsos [de], H. Yang [aj], S. Yasnopolskiy [o], J. Yi [bz], Z. Yin [bo], H. Yokoyama [by], I.-K. Yoo [bz], J. Yoon [cz], W. Yu [ad], X. Yuan [bo], I. Yushmanov [o], C. Zach [az], C. Zampolli [g,30], S. Zaporozhets [aq], A. Zarochentsev [v], P. Závada [dd], N. Zaviyalov [bl], H. Zbroszczyk [cq], P. Zelnicek [bi], I. Zgura [ce], M. Zhalov [av], X. Zhang [bo,1], D. Zhou [bo], F. Zhou [bo], Y. Zhou [bw], X. Zhu [bo], A. Zichichi [i,31], A. Zimmermann [bm], G. Zinovjev [r], Y. Zoccarato [bu], M. Zynovyev [r]

[a] Department of Physics and Technology, University of Bergen, Bergen, Norway
[b] Lawrence Livermore National Laboratory, Livermore, CA, United States
[c] Centro de Aplicaciones Tecnológicas y Desarrollo Nuclear (CEADEN), Havana, Cuba
[d] Nuclear Physics Institute, Academy of Sciences of the Czech Republic, Řež u Prahy, Czech Republic
[e] Yale University, New Haven, CT, United States
[f] Physics Department, Panjab University, Chandigarh, India
[g] European Organization for Nuclear Research (CERN), Geneva, Switzerland
[h] KFKI Research Institute for Particle and Nuclear Physics, Hungarian Academy of Sciences, Budapest, Hungary
[i] Dipartimento di Fisica dell'Università and Sezione INFN, Bologna, Italy
[j] Instituto de Física, Universidad Nacional Autónoma de México, Mexico City, Mexico
[k] Variable Energy Cyclotron Centre, Kolkata, India
[l] Department of Physics Aligarh Muslim University, Aligarh, India
[m] Gangneung-Wonju National University, Gangneung, South Korea
[n] Institute for Theoretical and Experimental Physics, Moscow, Russia
[o] Russian Research Centre Kurchatov Institute, Moscow, Russia
[p] Sezione INFN, Turin, Italy
[q] Centro Fermi – Centro Studi e Ricerche e Museo Storico della Fisica "Enrico Fermi", Rome, Italy
[r] Bogolyubov Institute for Theoretical Physics, Kiev, Ukraine
[s] Faculty of Engineering, Bergen University College, Bergen, Norway
[t] Frankfurt Institute for Advanced Studies, Johann Wolfgang Goethe-Universität Frankfurt, Frankfurt, Germany
[u] Dipartimento Interateneo di Fisica 'M. Merlin' and Sezione INFN, Bari, Italy
[v] V. Fock Institute for Physics, St. Petersburg State University, St. Petersburg, Russia
[w] National Institute for Physics and Nuclear Engineering, Bucharest, Romania
[x] Research Division and ExtreMe Matter Institute EMMI, GSI Helmholtzzentrum für Schwerionenforschung, Darmstadt, Germany
[y] Institut für Kernphysik, Westfälische Wilhelms-Universität Münster, Münster, Germany
[z] Rudjer Bošković Institute, Zagreb, Croatia
[aa] Sezione INFN, Padova, Italy
[ab] Sezione INFN, Bologna, Italy
[ac] SUBATECH, Ecole des Mines de Nantes, Université de Nantes, CNRS-IN2P3, Nantes, France
[ad] Institut für Kernphysik, Johann Wolfgang Goethe-Universität Frankfurt, Frankfurt, Germany
[ae] Laboratoire de Physique Subatomique et de Cosmologie (LPSC), Université Joseph Fourier, CNRS-IN2P3, Institut Polytechnique de Grenoble, Grenoble, France
[af] Departamento de Física de Partículas and IGFAE, Universidad de Santiago de Compostela, Santiago de Compostela, Spain
[ag] Oak Ridge National Laboratory, Oak Ridge, TN, United States
[ah] Helsinki Institute of Physics (HIP) and University of Jyväskylä, Jyväskylä, Finland
[ai] Sezione INFN, Catania, Italy
[aj] Commissariat à l'Energie Atomique, IRFU, Saclay, France
[ak] Laboratoire de Physique Corpusculaire (LPC), Clermont Université, Université Blaise Pascal, CNRS-IN2P3, Clermont-Ferrand, France
[al] Institute of Experimental Physics, Slovak Academy of Sciences, Košice, Slovakia
[am] Institute of Physics, Bhubaneswar, India
[an] Dipartimento di Fisica e Astronomia dell'Università and Sezione INFN, Catania, Italy
[ao] School of Physics and Astronomy, University of Birmingham, Birmingham, United Kingdom
[ap] The Henryk Niewodniczanski Institute of Nuclear Physics, Polish Academy of Sciences, Cracow, Poland
[aq] Joint Institute for Nuclear Research (JINR), Dubna, Russia
[ar] Niels Bohr Institute, University of Copenhagen, Copenhagen, Denmark
[as] Institut Pluridisciplinaire Hubert Curien (IPHC), Université de Strasbourg, CNRS-IN2P3, Strasbourg, France
[at] University of Houston, Houston, TX, United States
[au] Dipartimento di Fisica Sperimentale dell'Università and Sezione INFN, Turin, Italy
[av] Petersburg Nuclear Physics Institute, Gatchina, Russia
[aw] Physics Department, University of Jammu, Jammu, India
[ax] Laboratori Nazionali di Frascati, INFN, Frascati, Italy
[ay] Dipartimento di Fisica dell'Università and Sezione INFN, Padova, Italy
[az] Faculty of Nuclear Sciences and Physical Engineering, Czech Technical University in Prague, Prague, Czech Republic
[ba] Nikhef, National Institute for Subatomic Physics, Amsterdam, Netherlands
[bb] Centro de Investigaciones Energéticas Medioambientales y Tecnológicas (CIEMAT), Madrid, Spain
[bc] Department of Physics, Ohio State University, Columbus, OH, United States
[bd] Moscow Engineering Physics Institute, Moscow, Russia
[be] Institute for High Energy Physics, Protvino, Russia
[bf] Faculty of Science, P.J. Šafárik University, Košice, Slovakia
[bg] Wayne State University, Detroit, MI, United States
[bh] Saha Institute of Nuclear Physics, Kolkata, India
[bi] Kirchhoff-Institut für Physik, Ruprecht-Karls-Universität Heidelberg, Heidelberg, Germany
[bj] Institut de Physique Nucléaire d'Orsay (IPNO), Université Paris-Sud, CNRS-IN2P3, Orsay, France
[bk] Faculty of Mathematics, Physics and Informatics, Comenius University, Bratislava, Slovakia
[bl] Russian Federal Nuclear Center (VNIIEF), Sarov, Russia
[bm] Physikalisches Institut, Ruprecht-Karls-Universität Heidelberg, Heidelberg, Germany
[bn] Physics Department, University of Cape Town, iThemba LABS, Cape Town, South Africa
[bo] Hua-Zhong Normal University, Wuhan, China
[bp] Sección Física, Departamento de Ciencias, Pontificia Universidad Católica del Perú, Lima, Peru
[bq] Dipartimento di Fisica dell'Università and Sezione INFN, Trieste, Italy
[br] Centro de Investigación y de Estudios Avanzados (CINVESTAV), Mexico City and Mérida, Mexico
[bs] Dipartimento di Fisica dell'Università and Sezione INFN, Cagliari, Italy

[bt] Physics Department, Creighton University, Omaha, NE, United States
[bu] Université de Lyon, Université Lyon 1, CNRS/IN2P3, IPN-Lyon, Villeurbanne, France
[bv] Universidade Estadual de Campinas (UNICAMP), Campinas, Brazil
[bw] Nikhef, National Institute for Subatomic Physics and Institute for Subatomic Physics of Utrecht University, Utrecht, Netherlands
[bx] Division of Experimental High Energy Physics, University of Lund, Lund, Sweden
[by] University of Tsukuba, Tsukuba, Japan
[bz] Pusan National University, Pusan, South Korea
[ca] Sezione INFN, Cagliari, Italy
[cb] Benemérita Universidad Autónoma de Puebla, Puebla, Mexico
[cc] Dipartimento di Scienze e Tecnologie Avanzate dell'Università del Piemonte Orientale and Gruppo Collegato INFN, Alessandria, Italy
[cd] Instituto de Ciencias Nucleares, Universidad Nacional Autónoma de México, Mexico City, Mexico
[ce] Institute of Space Sciences (ISS), Bucharest, Romania
[cf] Universidade de São Paulo (USP), São Paulo, Brazil
[cg] Dipartimento di Fisica 'E.R. Caianiello' dell'Università and Gruppo Collegato INFN, Salerno, Italy
[ch] Sezione INFN, Bari, Italy
[ci] Soltan Institute for Nuclear Studies, Warsaw, Poland
[cj] Sezione INFN, Rome, Italy
[ck] Department of Physics, University of Oslo, Oslo, Norway
[cl] Lawrence Berkeley National Laboratory, Berkeley, CA, United States
[cm] Institute for Nuclear Research, Academy of Sciences, Moscow, Russia
[cn] Sezione INFN, Trieste, Italy
[co] Physics Department, University of Athens, Athens, Greece
[cp] Chicago State University, Chicago, United States
[cq] Warsaw University of Technology, Warsaw, Poland
[cr] Universidad Autónoma de Sinaloa, Culiacán, Mexico
[cs] Physics Department, University of Rajasthan, Jaipur, India
[ct] Technical University of Split FESB, Split, Croatia
[cu] Yerevan Physics Institute, Yerevan, Armenia
[cv] University of Tokyo, Tokyo, Japan
[cw] Department of Physics, Sejong University, Seoul, South Korea
[cx] Indian Institute of Technology, Mumbai, India
[cy] Institut für Kernphysik, Technische Universität Darmstadt, Darmstadt, Germany
[cz] Yonsei University, Seoul, South Korea
[da] Zentrum für Technologietransfer und Telekommunikation (ZTT), Fachhochschule Worms, Worms, Germany
[db] California Polytechnic State University, San Luis Obispo, CA, United States
[dc] China Institute of Atomic Energy, Beijing, China
[dd] Institute of Physics, Academy of Sciences of the Czech Republic, Prague, Czech Republic
[de] The University of Texas at Austin, Physics Department, Austin, TX, United States
[df] University of Tennessee, Knoxville, TN, United States
[dg] Dipartimento di Fisica dell'Università 'La Sapienza' and Sezione INFN, Rome, Italy
[dh] Hiroshima University, Hiroshima, Japan
[di] Budker Institute for Nuclear Physics, Novosibirsk, Russia
[dj] Laboratori Nazionali di Legnaro, INFN, Legnaro, Italy
[dk] Purdue University, West Lafayette, IN, United States
[dl] Centre de Calcul de l'IN2P3, Villeurbanne, France

* Corresponding author.
   E-mail address: andrew.adare@yale.edu (A.M. Adare).
[1] Also at Laboratoire de Physique Corpusculaire (LPC), Clermont Université, Université Blaise Pascal, CNRS-IN2P3, Clermont-Ferrand, France.
[2] Also at Sezione INFN, Bologna, Italy.
[3] Now at Physikalisches Institut, Ruprecht-Karls-Universität Heidelberg, Heidelberg, Germany.
[4] Now at Laboratoire de Physique Corpusculaire (LPC), Clermont Université, Université Blaise Pascal, CNRS-IN2P3, Clermont-Ferrand, France.
[5] Also at Dipartimento di Fisica dell'Universita, Udine, Italy.
[6] Now at Sezione INFN, Turin, Italy.
[7] Also at Benemérita Universidad Autónoma de Puebla, Puebla, Mexico.
[8] Also at European Organization for Nuclear Research (CERN), Geneva, Switzerland.
[9] Also at European Organization for Nuclear Research (CERN), Geneva, Switzerland.
[10] Now at Lawrence Berkeley National Laboratory, Berkeley, CA, United States.
[11] Now at Centro Fermi – Centro Studi e Ricerche e Museo Storico della Fisica "Enrico Fermi", Rome, Italy.
[12] Now at Warsaw University of Technology, Warsaw, Poland.
[13] Also at Fachhochschule Köln, Köln, Germany.
[14] Also at Institute of Experimental Physics, Slovak Academy of Sciences, Košice, Slovakia.
[15] Also at M.V. Lomonosov Moscow State University, D.V. Skobeltsyn Institute of Nuclear Physics, Moscow, Russia.
[16] Also at Laboratoire de Physique Subatomique et de Cosmologie (LPSC), Université Joseph Fourier, CNRS-IN2P3, Institut Polytechnique de Grenoble, Grenoble, France.
[17] Now at Dipartimento Interateneo di Fisica 'M. Merlin' and Sezione INFN, Bari, Italy.
[18] Now at SUBATECH, Ecole des Mines de Nantes, Université de Nantes, CNRS-IN2P3, Nantes, France.
[19] Also at "Vinča" Institute of Nuclear Sciences, Belgrade, Serbia.
[20] Also at Instituto de Ciencias Nucleares, Universidad Nacional Autónoma de México, Mexico City, Mexico.
[21] Now at Wayne State University, Detroit, MI, United States.
[22] Now at Department of Physics, University of Oslo, Oslo, Norway.
[23] Now at Eberhard Karls Universität Tübingen, Tübingen, Germany.
[24] Now at Research Division and ExtreMe Matter Institute EMMI, GSI Helmholtzzentrum für Schwerionenforschung, Darmstadt, Germany.
[25] Now at Institut Pluridisciplinaire Hubert Curien (IPHC), Université de Strasbourg, CNRS-IN2P3, Strasbourg, France.
[26] Also at Centro de Investigaciones Energéticas Medioambientales y Tecnológicas (CIEMAT), Madrid, Spain.
[27] Now at University of Tokyo, Tokyo, Japan.

[28] Also at Nuclear Physics Institute, Academy of Sciences of the Czech Republic, Řež u Prahy, Czech Republic.

[29] Also at Hua-Zhong Normal University, Wuhan, China.

[30] Now at Sezione INFN, Bologna, Italy.

[31] Also at Centro Fermi – Centro Studi e Ricerche e Museo Storico della Fisica "Enrico Fermi", Rome, Italy.